Available online at www.sciencedirect.com
SCIENCE DIRECT®
Composites: Part A 35 (2004) 619–629
composites
Part A: applied science and manufacturing
www.elsevier.com/locate/compositesa

Isothermal forging of AA2618 reinforced with 20% of alumina particles

P. Cavaliere*

INFM, Department of Ingegneria dell'Innovazione, Faculty of Engineering, University of Lecce, Via per Arnesano, I-73100 Lecce, Italy

Received 7 October 2002; revised 13 October 2003; accepted 25 February 2004

Abstract

The isothermal forming behaviour of AA2618 + 20% Al_2O_3 has been studied by hot-torsion and hot-compression tests. The constitutive equations and the strain rate sensitivity coefficient of the investigated composite were estimated from flow stress curves. The strain rate sensitivity coefficient reached the highest values in the temperature and strain rate ranges of 450–500 °C and 10^{-2}–10^{-1} s^{-1}, respectively. The microstructural evolution of the material during deformation was studied by optical and scanning electron microscopy. The degree of material damage was evaluated in terms of matrix–particle decohesion and particles fracture. A three-dimensional FEM modelling of a real industrial component was performed in order to determine the best forging conditions. This component was isothermally forged under the process conditions derived by the FEM simulations, a defect free product was thus obtained.

Keywords: Aluminium based metal matrix composites; Isothermal forging; Damaging; FEM

1. Introduction

The strong pressure for weight reduction in car and aircraft fabrication urges the optimisation of the design of products employing low weight materials. The replacement of conventional materials by lighter metals such as aluminium alloys is, therefore, highly desirable. However, aluminium alloys are not sufficiently stiff or strong for many purposes and their reinforcement is necessary. Aluminium based metal matrix composites (Al-MMCs) are outstanding candidates for these applications owing to the high ductility of the matrix and the high strength of the hard reinforcing phases. Unfortunately, such materials are difficult to form due to their intrinsic poor ductility caused by the presence of the undeformable reinforcing phase, usually SiC or Al_2O_3 particles. As a matter of fact, previous investigations on hot formability of metal matrix composites (MMCs) typically show unacceptable degrees of damaging associated with the matrix–particle decohesion and particle fracture. These failure modes are due to two chief mechanisms: (i) high concentration of dislocations at the matrix–particle interfaces, (ii) void growth originating from microvoids generated during prior thermomechanical history of the material [1–6]. Embury and co-workers demonstrated that damage initiation is governed by particle size, particle aspect ratio and spatial distribution [7]. Mummery et al. [8] and Lewandowski and co-workers [9,10] have experimentally shown the effect of morphology and matrix properties on reinforcement fracture and interfacial decohesion. Studies by Li and Ellyin [11] revealed different damage mechanisms, in terms of particle debonding and fracture or matrix cracking, as a function of forming conditions in alumina-reinforced aluminium.

Consequently, the proper selection of the forming parameters critically affects the production of sound components. Forming conditions can be more easily optimised if experimental and numerical models are available, that describe the evolution of damage. Workability describes the ability of the material to be shaped by plastic flow without fracture and it is strongly influenced by the processing parameters, such as temperature and strain rate, which also affect the microstructural development during hot forming processes [1–5]. Even though in some forming processes, the stress state is essentially compressive or tensile, practical stress fields generally exhibit stress components that can be compressive or tensile in the same workpiece. As a consequence, it is difficult to estimate the workability because of all the variables, which play a role during deformation. For this reason, several

* Tel.: +39-0832320349; fax: +39-0832320324.
E-mail address: pasquale.cavaliere@unile.it (P. Cavaliere).

1359-835X/$ - see front matter © 2004 Elsevier Ltd. All rights reserved.
doi:10.1016/j.compositesa.2004.02.014

simple laboratory tests have been developed to simulate the stress state taking place within the workpiece during deformation.

The design and control of forming processes depend on a large number of parameters among which: material properties, environmental conditions, thermomechanical parameters, mechanics of plastic deformation and equipment used. Another important aspect is the frictional behaviour of the workpiece–die interfaces. Because of the large surfaces in contact, very high friction forces can be developed during forging processes; such forces can be reduced by using appropriate lubricants.

Hot-torsion and -compression tests can be conveniently used to study the plastic deformation of a material under different conditions of temperature and strain rates. Moreover, they allow simulating the isothermal conditions occurring in some industrial forming processes. In fact, isothermal forging of Al-MMCs has the potential to manufacture components characterised by low damage levels. This technology seems to be the most promising for these purposes [12–14]. Several investigations were published on the hot forming of Al-MMCs; in particular, the constitutive equations relating flow stress, temperature and strain rates, have been analysed in order to correlate the mechanical response to the microstructural evolution in terms of grain size, dislocation distribution and damage. Roberts and co-workers studied the hot-compression behaviour of Al-MMCs relating the composites damage in terms of: (i) number of voids per mm^2, (ii) percent of area of the voids respect to the total section of the specimen as a function of hot-compression parameters (temperature and strain rate) and (iii) particles fracture, by using optical and electron microscopy techniques [15,16]. They also studied the influence of particles size and distribution (clustering), on damage levels; in particular they demonstrated a change in damage mechanisms from particles fracture to void formation as a function of the degree of particles clustering [17]. Other scientists published some papers regarding the debonding and damage behaviour of ceramic-reinforced MMC using tomography techniques and finite element modelling [18–21].

In order to implement MMCs on a wide scale in the modern industry significant effort is still required to understand the relationship between processing and in service behaviour. In particular, the forging route would provide a significant improvement in the elongation properties of the material, thereby making it less susceptible to fracture with respect to its cast counterpart. At the same time, the forging process imparts localised damage in some areas of the workpiece, with an associated detrimental effect on properties. The complex interaction among temperature, strain, strain-rate, stress and microstructure make physical modelling of damage accumulation during processing difficult. Approaches such as the 'critical strain-rate' criterion of Humphreys and Kalu and calculations of the stress in and around the particle using the methods of Mori and Onaka, have been attempted with some success. These methods have given some indication of the areas in a forging susceptible to damage but have so far failed to predict a priori the absolute values of damage levels. The increasing application of FEM methods to materials science problems makes it possible to simulate forming processes and furthermore to determine the strain, strain rate and damage distribution within the forged parts. In this paper, the best-practice forging conditions obtained by laboratory tests, have been used to model the material behaviour by using a 3D FEM code. Subsequently, a practical component used in the aeronautic industry was produced in isothermal conditions obtaining a defect free product. Specifically, the aim of the present work is the characterisation of the hot formability of AA2618 + 20% Al_2O_3 in isothermal conditions in order to correlate the forming parameters to the microstructural evolution in terms of damage mechanisms, dynamic recovery and recrystallisation (DRX) [22–27]. The microstructural damage of the material has been evaluated in terms of area of the voids/total area of the specimen in order to calculate the reduction of the resistant section to the applied stress after the thermomechanical processing of the material. The damage levels were evaluated in all the isothermal forming conditions investigated by scanning electron microscopy technique (SEM).

2. Experimental procedures

The material investigated (AA2618 + 20% Al_2O_3) was produced by DURALCAN (USA) by mixing 20% of Al_2O_3 particles into a molten AA2618 aluminium alloy. After casting, billets were pre-homogenised at 570 °C for 4 h and cooled to room temperature at 200 °C/h. Then, the billets were hot extruded into 80 mm diameter rods. The matrix used in the present work had the following chemical composition (wt%): Cu = 2.3%, Mg = 1.6%, Fe = 1.1%, Ni = 1.0%, Ti = 0.07%, Si = 0.18%, Al = bal. The average size of the Al_2O_3 particles was about 10 μm.

The damage of the material caused by the extrusion process was evaluated by SEM-FEG and quantified as percent of the void area with respect to the total section of the specimen (Table 1).

Isothermal compression tests were carried out using a servohydraulic testing machine (MTS 810).Cylindrical samples with an initial height (h_0) and diameter (d_0) of 18 and 12 mm, respectively, were used in order to obtain

Table 1
Damage of the materials in terms of area of the voids (%) normalized to the total area of the specimen in the as-received condition

Composite	Section	Area of the voids (%)/total area of the specimen
2618/20% Al_2O_3	Longitudinal	6.70
2618/20% Al_2O_3	Transverse	7.40

the true stress–true strain curves. The specimens were compressed up to a height reduction of 50%, in isothermal conditions in the temperature and strain rate ranges of 350–500 °C and 10^{-3}–1 s^{-1}, respectively. The sample-die interface was lubricated with molybdenum disulphide.

Light microscopy, scanning electronic microscopy and computer image analysis have been used to quantify the microstructural damage in the deformed samples. The samples were prepared for metallographic observations by grinding consecutively on 360, 600, 800, 1000, 2400 and 4000 SiC papers, and then polished on 3 μm diamonds cloths. The samples were etched with Keller's reagent in order to show the grain size developed by dynamic recovery or recrystallisation. The samples subjected to compression-tests were analysed in the core region parallel to the compression axis, whilst the torsion-tested ones were ground on the gage surface parallel to the torsion axis where the strain is the maximum. A set of samples was also cut from the forged component in order to evaluate the grain size evolution and damage mechanisms developed during forming operations.

3. Results and discussion

3.1. Mechanical testing and constitutive equations

The applied load (P) versus ram linear displacement (Δh) were converted to true stress (σ) versus true strain (ε) values by means of the following relationships:

$$\sigma = \frac{P(h_0 - \Delta h)}{A_0 h_0} \tag{1}$$

$$\varepsilon = \ln\left(\frac{h_0}{h_0 - \Delta h}\right) \tag{2}$$

where A_0 and h_0 are the initial cross-sectional area and the height of the sample, respectively.

The true stress (σ) was subsequently corrected for friction according to the slab analysis of the compression of a cylinder with a constant friction shear factor (f), the value chosen for the present study was $f = 0.3$ [28,29]:

$$p = \sigma\left[1 + \frac{fd_0}{3\sqrt{3}h_0}\exp(\varepsilon)^{1.5}\right] \tag{3}$$

The compression curves are illustrated in Fig. 1 at different strain rates (Fig. 1(a)) and temperatures (Fig. 1(b)). The flow curves show a classical behaviour with a net increase in stress with strain up to the maximum, followed by a limited flow softening. The flow stress of the material increases with increasing strain rate and decreasing temperature.

Torsion tests were carried out in the same temperature and strain rate ranges as the hot-compression tests. The samples were heated using an induction furnace;

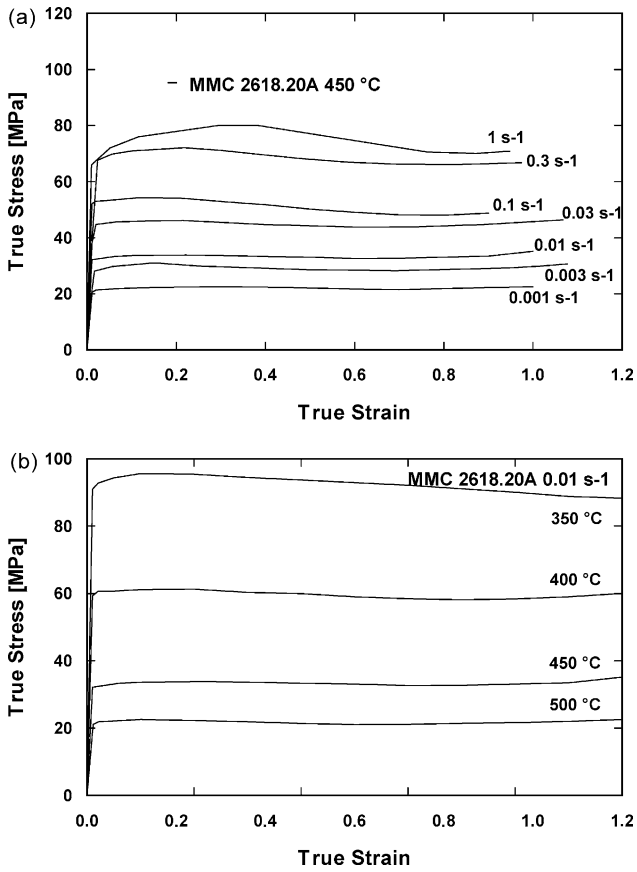

Fig. 1. True stress (MPa) versus true strain hot-compression curves of AA2618 + 20% Al_2O_3 MMC at various strain rate and temperatures.

the temperature stabilisation time was 6 min. The gauge section of samples was a solid cylinder with a length (L) of 7 mm, and a radius (R) of 4 mm; the fillet radius between the gauge section and the shoulders was 0.5 mm. The torque (Γ) and the twist angle (θ) were converted to surface shear stress (τ) and strain (γ) with the relationships:

$$\tau = \frac{\Gamma}{2\pi\pi^3}(3 + n' + m') \qquad \gamma = \frac{R\theta}{L} \tag{4}$$

where n' ($= \mathrm{dlog}\,\Gamma \log \Gamma/\theta|_{\dot{\theta},T}$) is the work hardening rate and m' ($= \mathrm{dlog}\,\Gamma \log \Gamma/\dot{\theta}|_{\theta,T}$) is the revolution rate sensitivity coefficient of torque. Equivalent stresses (σ) and strains (ε) were derived from surface shear stresses and strains by means of the Von Mises yield criterion [30,31]:

$$\sigma = \tau\sqrt{3} \qquad \varepsilon = \gamma/\sqrt{3} \tag{5}$$

Because of the temperature increase (ΔT) due to the deformation heating, the flow curves for $\varepsilon \geq 10^{-1}$ s^{-1} did not correspond to isothermal conditions. Therefore, a temperature correction was applied to flow stress under such conditions. For each value of equivalent strain, the temperature increase was calculated using the following

relationship:

$$\Delta T = \frac{B\int_0^{\varepsilon}\sigma\,\mathrm{d}\varepsilon}{\rho c} \tag{6}$$

where β is the deformation heat factor, ρ is the material density, and c is the heat capacity.

The temperature increase was used to offset flow-softening effects due to the deformation heating by correcting flow stress employing the equation:

$$\sigma_c = \sigma + \Delta\sigma = \sigma + \Delta T\frac{\mathrm{d}\sigma}{\mathrm{d}T} \tag{7}$$

where σ_c is the flow stress corrected for the deformation heating.

The torsion flow curves are characterised by an increase in flow stress with strain up to a peak followed by a steady state or by a very limited slight softening until fracture occurs, as shown in Fig. 2. By analysing the true stress–true strain curves in torsion and compression, it results that the flow stress in compression is higher ($\approx 10\%$) than that in torsion [29]. The torsion stress–strain curves show consistently lower levels of flow stress because of different reasons such as the effect of deformation path different microstructure transformations and in particular lower levels of strain hardening. This effect is more evident at the lower temperatures investigated during tests [28–32].

The ductility is quantified as strain to fracture versus temperature at different strain rates. In the range investigated, ductility increases with increasing temperature and decreasing strain rate (Fig. 3).

The isothermal forming behaviour of AA2618 + 20% Al_2O_3 was subsequently modelled by correlating flow stress to strain rate and temperature according to the well known constitutive equation [33–35]:

$$Z = \dot{\varepsilon}\exp(Q/RT) = A[\sinh(\alpha\sigma)]^n \tag{8}$$

where Z is the Zener–Hollomon parameter representing the temperature-modified strain rate, Q is the activation energy for deformation, R is the universal gas constant, T is the absolute temperature, $\dot{\varepsilon}$ is the strain rate, A, n and α are material parameters.

The activation energy was calculated by the relationship:

$$Q = -R\left.\frac{\partial \ln\dot{\varepsilon}}{\partial(1/T)}\right|_{\sigma} = 2.3R\left.\frac{\partial\log\dot{\varepsilon}}{\partial\log\sinh(\alpha\sigma)}\right|_{\varepsilon,T}\left.\frac{\partial\log\sinh(\alpha\sigma)}{\partial(1000/T)}\right|_{\varepsilon,\dot{\varepsilon}} = 2.3Rns \tag{9}$$

The slopes of $\log(\dot{\varepsilon}) - \log[\sinh(\alpha\sigma)]$ at constant T and $\log[\sinh(\alpha\sigma)] - 1000/T$ at constant strain rates were calculated, leading to a value of the activation energy of 186 kJ/mol. The value of the stress multiplier α was calculated by means of an optimisation procedure and $\alpha = 0.02\,(\mathrm{MPa})^{-1}$ gave the best correlation coefficient for the linear relationships $\log(\dot{\varepsilon}) - \log[\sinh(\alpha\sigma)]$

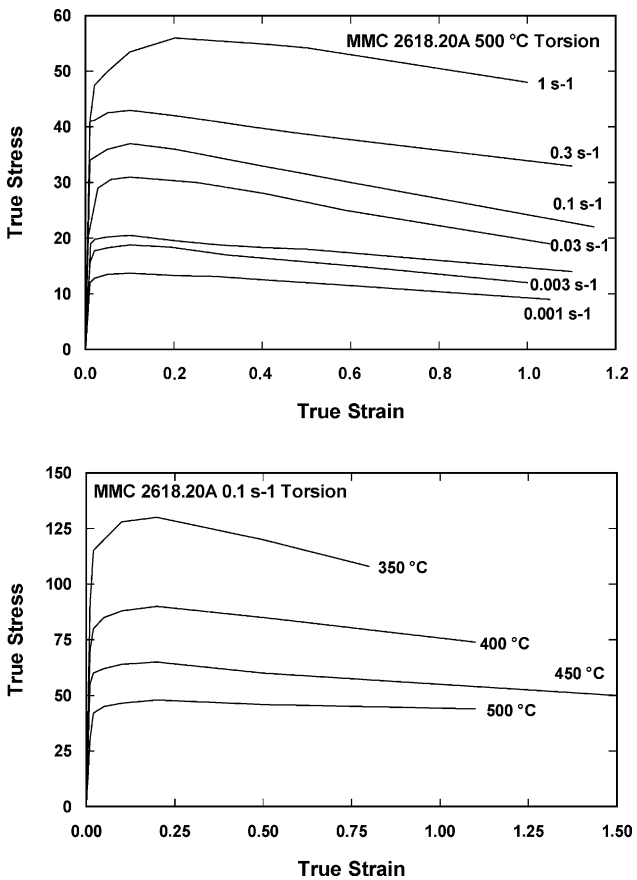

Fig. 2. True stress (MPa) versus true strain hot torsion curves of AA2618 + 20% Al_2O_3 MMC at various strain rate and temperatures.

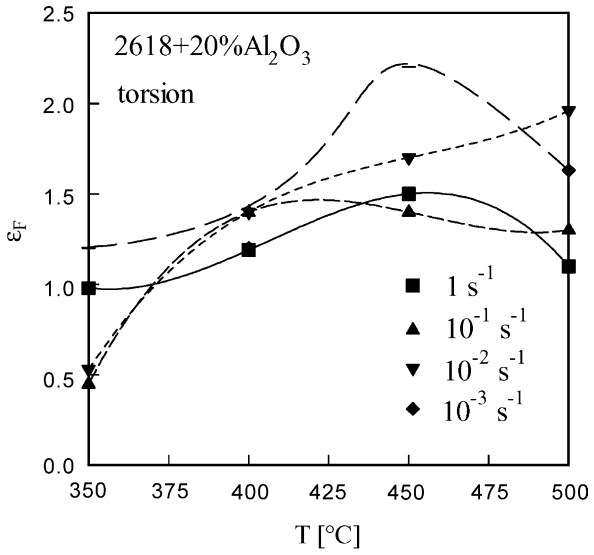

Fig. 3. Plots of strain to fracture as a function of temperature and strain rate showing the ductility of the AA2618 + 20% Al_2O_3 MMC obtained by torsion tests.

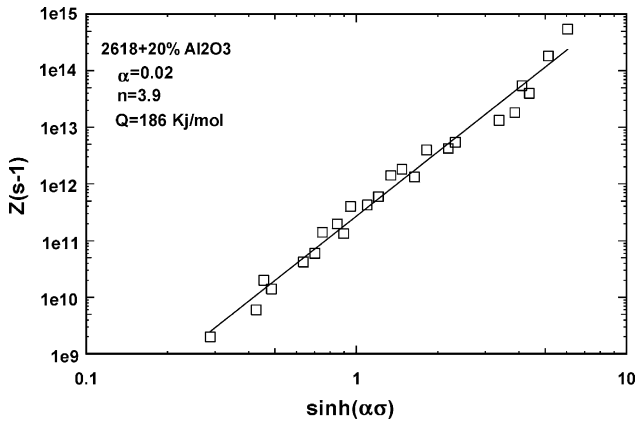

Fig. 4. Zener–Hollomon parameter plotted as a function of flow stress for the AA2618 + 20% Al_2O_3 composite.

and $\log[\sinh(\alpha\sigma)] - 1000/T$. The calculation of the Zener–Hollomon parameter showed a good correlation for the compression and torsion test data by considering $Q = 186$ kJ/mol and $\alpha = 0.02\ (\text{MPa})^{-1}$ and is shown in Fig. 4.

The strain rate sensitivity coefficient (m) of the material was calculated employing the following equation [35–38]:

$$m = \left.\frac{\partial \log \sigma}{\partial \log \dot{\varepsilon}}\right|_{\varepsilon,T} \tag{10}$$

The m value was calculated by interpolating the data obtained by torsion and compression tests at an equivalent strain of 0.5 (Fig. 5). The cubic interpolation was applied between σ and $\dot{\varepsilon}$ logarithmic values [5,39–42]. The map obtained shows the variation of the strain rate sensitivity coefficient m with temperature and strain rate, giving the behaviour of the material in all the test conditions.

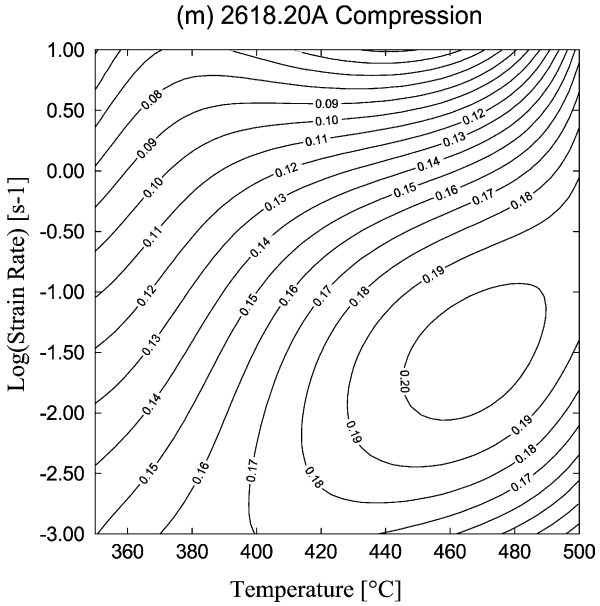

Fig. 5. Two-dimensional maps showing the strain rate sensitivity (m) as a function of temperature and strain rate for the studied material.

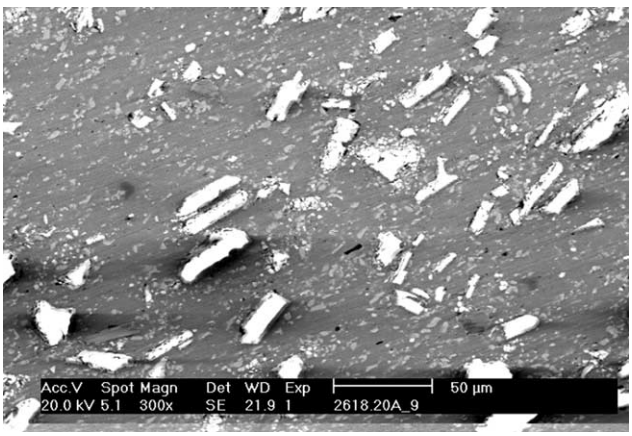

Fig. 6. SEM microstructure of the studied composite.

3.2. Microstructure and damage evaluation

The microstructure of the AA2618 + 20% Al_2O_3 in the as-extruded condition consists of fine equiaxed recrystallised grains with an average size of 10 μm and of a relatively high fraction of second-phase precipitates (Al_2CuMg), located both at the grain boundaries and inside the grains. The SEM microstructure of the as-received material is showed in Fig. 6. The 2618-aluminium alloy is age hardenable and can be strengthened through heat treatments, inducing a fine dispersion of precipitates giving rise to obstacles for dislocations motion. The addition of Fe and Ni favours the microstructural stability at temperatures up to 200 °C. The strength of the material is due to a combination of precipitation and dispersion hardening. The main precipitates were recognised as coherent Guinier–Preston–Bagaryatskii (GPB) (Cu, Mg) zones and semi-coherent S′ (Al_2CuMg) phase. The presence of stable intermetallic particles, such as aluminides (Al_9FeNi), favours the grain size control and inhibits the dislocation motion.

The microstructure of samples tested in compression at 500 °C and $\varepsilon = 10^{-2}\ \text{s}^{-1}$ ($\varepsilon = 1$) is shown in Fig. 7.

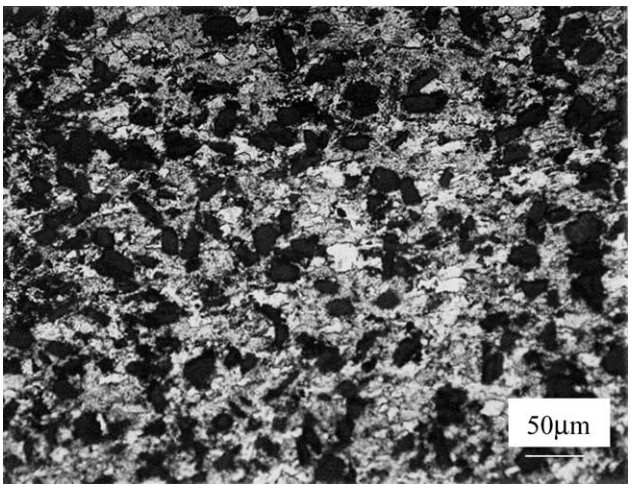

Fig. 7. Optical micrograph of hot-compression tested sample (500 °C, $10^{-2}\ \text{s}^{-1}$).

The uniform and fine grain size can be attributed to the occurrence of dynamic recrystallisation [21]. The most heavily deformed zone of the samples revealed chains of particles (intermetallic phases or fragmented reinforcement particles) aligned along the flow direction, but separated by equiaxed and undeformed grains. The size of the equiaxed grains at 500 °C is slightly larger than at 450 °C, whilst a reduction in strain rate at a given temperature results in a moderate increase in grain size. These phenomena have a straightforward physicak explanation. It has been known since the late 1950s or early 1960s that the flow curves associated with DRX are characterised by being cyclic or 'single peak'. It has been recently shown that single peak flow is associated with grain refinement [21,43,44]. The physical mechanisms governing DRX are very similar to those controlling static recrystallisation (SRX). Normally, aluminium alloys do not exhibit DRX because of their low hot worked dislocation densities, but nucleation and growth of new grains can indeed be induced in the presence of sufficient quantities of hard second phase, such as in composites reinforced with small particles [45]. These appear to raise the local dislocation densities and lattice curvatures above the critical levels needed for the initiation and propagation of DRX. It has long been established that recrystallisation is prevented or delayed by a dispersion of closely spaced second-phase particles, due to the pinning (Zener drag) of both high and low angle boundaries. During deformation, particles will affect the deformation microstructure through effects such as an increase in dislocation density, the production of large deformation heterogeneities at larger particles and the alteration of the homogeneity of slip, e.g. shear bands. During the deformation of a particle-containing alloy, the enforced strain gradient in the vicinity of a non-deforming particle creates a region of high dislocation density and large orientation gradient, which is an ideal site for the development of a recrystallisation nucleus [21]. It is well known that the resulting deformation zones extend to a distance of about a diameter from the surface of the particles and that they may be misoriented by tens of degrees from the adjacent matrix. Recent work on the deformation of particle-containing single crystals [44] has shown that, in addition to the lattice misorientations, small deformation bands may be formed very close to the particles and these can extend for more than 10 particle diameters. These bands are regions which are destabilised by the presence of the particle, and which rotate during deformation towards stable orientations. In particular, dynamic recovery leads to the formation of subgrain boundaries, which progressively transform at large strains into new large angle grain boundaries, a mechanism that has been referred to as continuous DRX. Under such mechanism, the material grain size decreases during straining. Geometric DRX is a process in which the high angle boundaries are forced together at large strains and elevated temperatures. At a critical strain, which is a function of the flow stress and the initial grain size, the spacing of the high-angle boundaries is reduced to the dimensions of the subgrain size, the high angle boundaries begin to touch and a new microstructure of mainly high angle boundaries is effectively formed [45–48]. It has been demonstrated that several metals, such as particles reinforced MMCs, develop a very fine grain structure classified as 'continuous recrystallization' when deformed at high temperature. Many authors have widely demonstrated that hot restoration mechanisms are favoured by the addition of ceramic reinforcements to aluminium alloys and in particular promoted the initiation of DRX during hot deformation by increasing dislocation density in the matrix [49,50].

The flow behaviour response of ceramic-reinforced MMCs is mainly governed by two processes: (i) the first one involves load transfer from the matrix to the particles, leading to an increase in flow-stress at the interfaces between the ductile matrix and the quasi-rigid particles; (ii) the second one involves the development of microstructural damage producing particle cracking or decohesion of the particle–matrix interface. Particle cracking occurs when the composite material is not able to dissipate the energy produced by the deformation through metallurgical transformations such as dynamic recovery or recrystallisation [50–53]. This process, in turn, is possible only

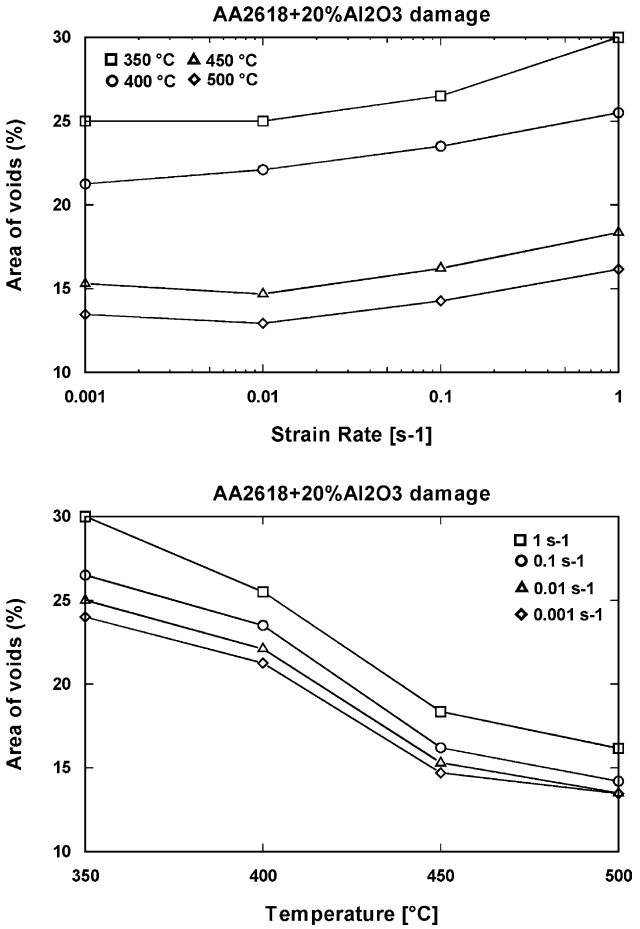

Fig. 8. Damage evolution of the studied material after hot-compression tests in all the investigated conditions.

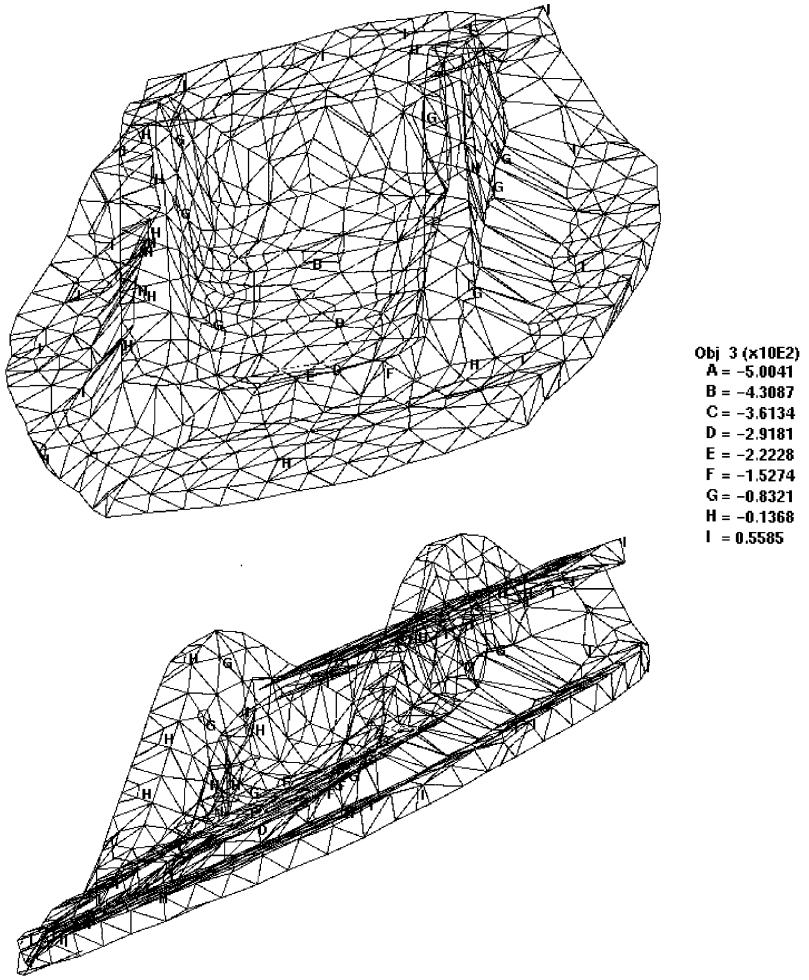

Fig. 9. Principal stress distribution in the component at the final step of the simulation for the AA2618 + 20% Al_2O_3 MMC.

when the particle–matrix interface is largely undamaged. On the other hand, particle cracking could lead to the macroscopic crack initiation up to the fracture. The same could be said for crack initiation at the interface between particles and matrix. Finally, also the nature of the load affects the material response: compressive stresses, in principle, should in fact retard crack propagation [54,55]. Decohesion at the particle–matrix was observed in all samples; the material damage in the deformed conditions was evaluated as a function of temperature and strain rate in all the investigated conditions. The images for the evaluation of the material damage were taken from the centre of the compression specimens deformed at a true strain value of ≈ 1. For every calculation, the mean area of the voids formed around 100 particles were considered. At all the temperatures investigated, the area of the voids decreases with decreasing strain rates until a value of $10^{-1}\ s^{-1}$. At 350, 400 and 450 °C, it starts to increase at a strain rate value of $10^{-2}\ s^{-1}$ (Fig. 8). The calculation of the strain rate sensitivity led to the conclusion that m increases with increasing temperature in the strain rate regime investigated. At the same time, it increases with decreasing strain rate up to a maximum observed in the range of 10^{-1}–$10^{-2}\ s^{-1}$. Many fractured particles were observed at 350 and 400 °C at all the strain rates investigated. In these deformation regimes, the matrix is not so ductile as to dissipate the stress but transfers a large part of the force to the particles with the consequence of the formation of large voids, accompanied with particles fracture.

3.3. FEM analysis and isothermal forging experiments

The FEM simulations of the isothermal forging of AA2618 + 20% Al_2O_3 were performed using a 3D numerical code with a rigid-visco-plastic formulation; the frictional shear stress (τ) was expressed as: $\tau = f\sigma$. The value of the friction factor was taken from Refs. [28,29]. The properties of the composite were determined experimentally assuming an isotropic continuum. At the macro-level, this is acceptable as the typical 10 μm diameter of the particulate is small in comparison with the scale of the studied component. The stress state in the forged components depends on the geometry of the deformation zones. The workpiece during deformation is subjected to a three-dimensional (3D) state of stress. This stress state is represented by a stress tensor with nine components or six

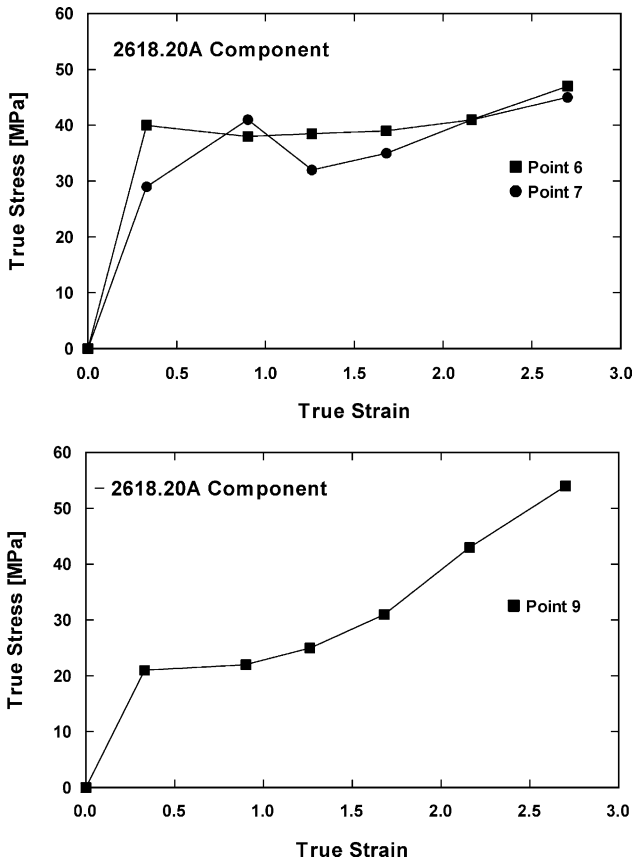

Fig. 10. True stress versus true strain curves in different points of the forged component.

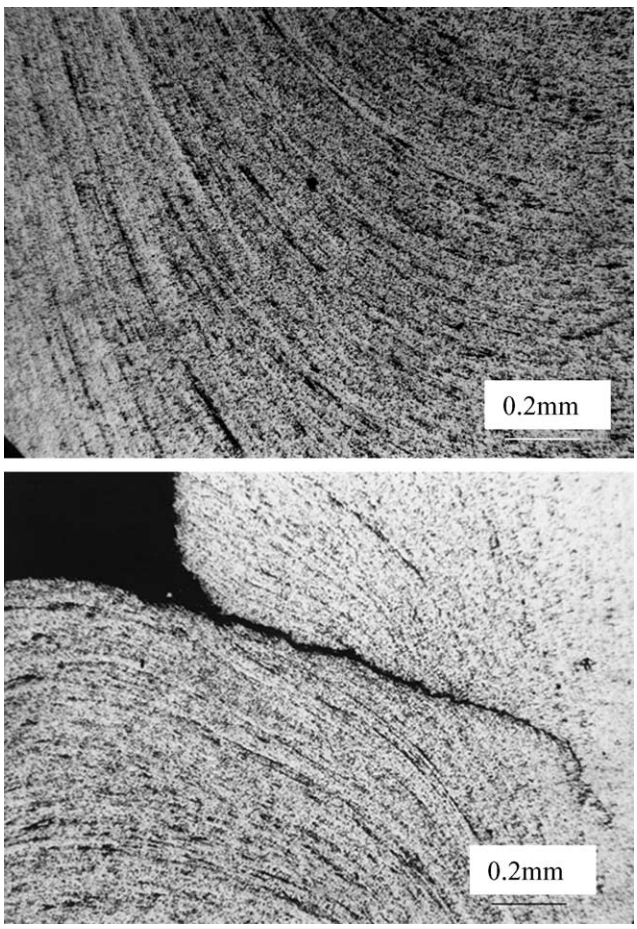

Fig. 11. Flow lines and fracture observed in the AA2618 + 20% Al_2O_3 MMC forged at 450 °C.

independent components. Three shear stress components contribute to the plastic flow of the material, whilst the hydrostatic components affect the workability. The stress state is specific of the forming process and is independent on the material behaviour. For this reason, FEM codes have been developed to predict the stress–strain state in different points of a complex geometry component [40,41]. The finite element analysis of the isothermal forging process was carried out using the DEFORM™ 3D FEM code, a general purpose program performing both elastic-plastic and rigid-plastic analyses.

The subdivision of subregions into a mesh system of eight-node hexahedral elements was performed automatically in the workpiece. Three-dimensional metal forming processes are characterized by a continuous shape modification of the workpiece. The simulations were performed by using the geometry of the real dies and of the billet; the computation was carried out with automatic remeshing; at every increment step. The method of modifying the node in contact with the die according to its original normal has been applied. In fact, this approach causes the initial FEM mesh to distort during the deformation to such a degree that a new FEM mesh system is necessary for the correct simulation. The step increments were saved at every mm of the stroke. After simulation, 10 points were chosen in the billet in order to perform the point tracking and follow the behaviour of stress, strain, strain rate and damage during the stroke of the dies. The flow data of AA2618 + 20% Al_2O_3, experimentally determined by compression tests, were given as input to the FEM code. The simulations were carried out at the temperatures of 450 and 500 °C and initial strain rates of 10^{-2} and 10^{-1} s^{-1}.

The principal stress can be a very good indicator of the material behaviour during forming operations; its distribution was obtained through the FEM simulations and mapped in different conditions of temperature and displacement. The highest value of the principal stress was 55 MPa (line I, Fig. 9) at 500 °C and initial strain rate of 10^{-2} s^{-1}. The negative values of the principal stress, in Fig. 9, represent the regions of the workpiece subjected to a compressive stress state during deformation. The stress distributions in the forged component were calculated in all the simulated conditions. The principal stress levels reached in the component during the simulations at 450 °C resulted higher than those observed at 500 °C. The forming curves were obtained in order to evaluate the possibility of forging the component in all the simulated conditions. The stress state in the component was examined, especially at the top.

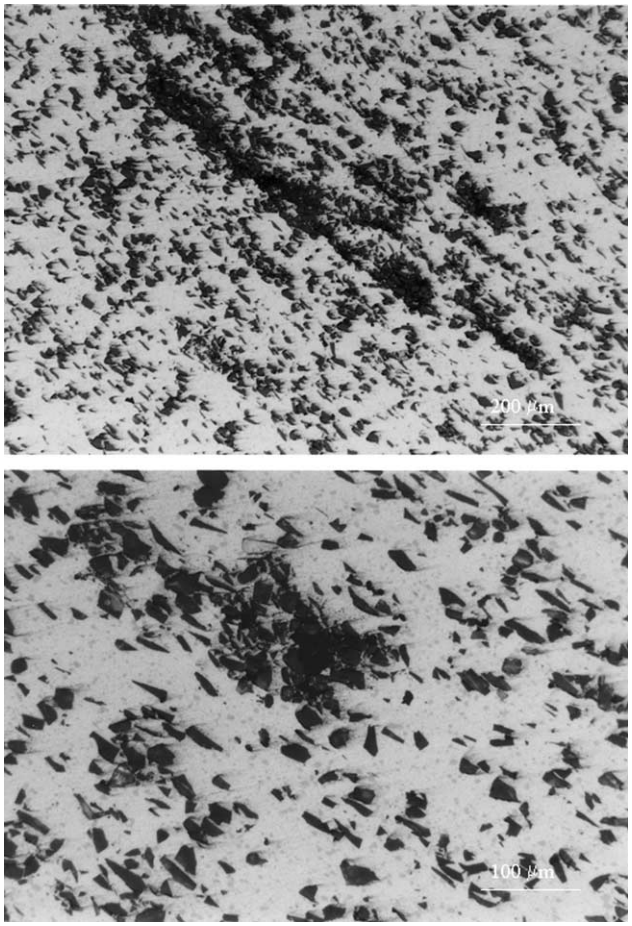

Fig. 12. Clusters of particles in the AA2618 + 20% Al_2O_3 MMC forged at 450 °C.

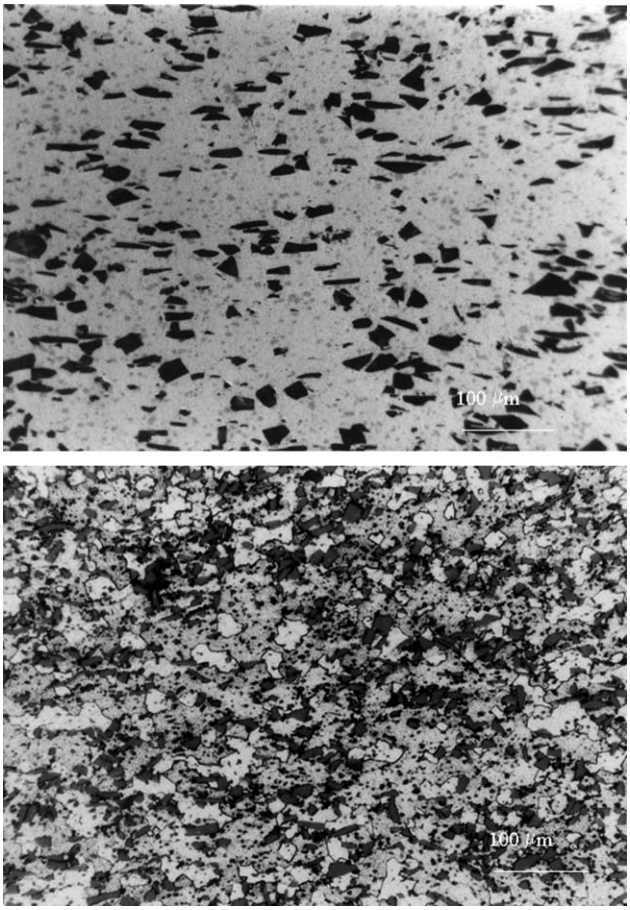

Fig. 13. Non-etched and etched microstructure of AA2618 + 20% Al_2O_3 MMC forged at 500 °C and 10^{-2} s^{-1}.

In fact, the stress reached 55 MPa in the simulations performed at 500 °C and 77 MPa at 450 °C. The same values were observed in the flash zone of the component. The stress versus strain curves were calculated for the points 6, 7, 9 in the component, as shown in Fig. 10. The points indicated with the number 9 correspond to the flash zone where the highest values are reached. The points 6 and 7 are those corresponding to the top of the component, where the stress state is quite similar to the maximum observed in the laboratory tests. The maximum stress values, reached during the isothermal forging of the component, are lower than those calculated from the simulation tests by torsion and compression.

3.4. Microstructure of the forged component

Finally, the MMC component, industrially produced by 2618 matrix alloy, was forged under isothermal conditions at temperatures of 450 and 500 °C and with an initial strain rate of 10^{-2} s^{-1} in order to evaluate the macro and microstructure of the material in these forming conditions The forging operations were carried out at the CSM Laboratories (Rome) by a 250 kN testing machine on specimens of 50 mm diameter and 35 mm height. The macro and microstructure of the isothermally forged components have been examined in detail. Some cross-sections of the component were observed in order to reveal the flow lines of the material during plastic deformation. The microstructure was observed in order to evaluate the void formation at the matrix–particle interface and grain evolution [14,22,31]. The flow lines were observed in the component forged at 450 °C. In the same component, an underfill of the die is shown (Fig. 11). For the materials deformed at 500 °C, this phenomenon was not present because of the higher ductility of the alloys at that temperature. At 500 °C, in fact, a homogeneous particle distribution and a more uniform microstructure were observed. The examination of the forged materials continued with the microscopic observation of non-etched samples of different sections of the component. Several fractured particles were observed in the component forged at 450 °C with the formation of particle clusters in the high strained zones (Fig. 12). These clusters inhibit the plastic flow of the material owing to a reduction of maximum stresses at the centre of the clustered particles and the high levels of hydrostatic stress in the clustered regions.

All this clusters are accompanied by void formation indicating large zones of stress concentration in the structure during forging. In these temperature conditions all the stress is transferred from the matrix to the particles which fracture when this stress reaches high values.

In the material tested at the temperature of 500 °C, this phenomenon is absent because the matrix ductility can be restored through various mechanisms such as DRX and recovery. The material is thus able to flow transferring the stress to the particles without fracture. The non-etched microstructure appears very uniform and without voids. The etched microstructure is characterised by small and uniformly distributed equiaxed grains, typical of DRX (Fig. 13). Normally in the unreinforced aluminium alloys DRX is absent at these temperatures, while in the composite, the reinforcing particles can act as nucleation sites. The particles play a fundamental role in controlling the grain size by particle-stimulated nucleation. If each particle produces one recrystallised grain, it is clear that a very large number of new nucleation sites are produced and so a lot of small new grains are achievable in these materials. The recrystallisation kinetics of particulate MMCs is usually very rapid compared to the unreinforced matrix. This is a combination of the large driving force due to the geometrically necessary dislocations and the large number of nucleation sites. In addition, the fine precipitate dispersion observed in this material promotes new nucleation sites for the recrystallisation phenomenon [21].

4. Conclusions

In the present work, the hot formability of a AA2618 + 20% Al_2O_3 composite was tested in torsion and compression at temperatures between 350 and 500 °C and strain rates between 10^{-3} and 1 s^{-1}. The flow-stress versus strain rate data obtained from the experiments were used to calculate the values of strain rate sensitivity in all the conditions of temperature and strain rates. Subsequently, the constitutive equations of the composite were determined and the microstructure was characterised by using optical and SEM techniques. The damage level of the material was then evaluated in all the deformation regimes in terms of reduction of the resistant section due to decohesion at the interfaces between the hard reinforcing particles and the ductile aluminium matrix. Optimal forging conditions were individuated in the temperature and strain rate ranges of 450–500 °C and 10^{-2}–10^{-1} s^{-1}, respectively. In these conditions, by using a FEM 3D numerical code the simulation of isothermal forging of a complex component was performed in order to evaluate the stress distributions in different points of the trial. Afterwards, the component was isothermally forged with good results in terms of die filling and microstructure at 500 °C and 10^{-2} s^{-1}.

References

[1] Sakaris P, McQueen HJ. Comparative hot workability of SiCp/A356 and SiCp/6061 Al composites and their matrices. In: Avedesian MM, Larouche LJ, Masounave J, editors. Advances in production and fabrication of light metals (Edmonton). CMI Montreal; 1992. p. 605–17.
[2] De Sanctis AM, Evangelista E, Forcellese A. Assesment of the forging conditions of 6061/Al_2O_3/10p using processing maps and stability criteria. Engineering materials, vols. 127–131. Switzerland: Trans Tech Publications Ltd; 1997. p. 525–32.
[3] Lloyd DJ. Particle reinforced aluminium and magnesium matrix composites. Int Mater Rev 1994;39:123.
[4] McQueen HJ, Jonas JJ. In: Hoffmanner AL, editor. Metal forming: interrelation between theory and practice. New York: Plenum Press; 1971. p. 393.
[5] De Sanctis AM, Evangelista E, Forcellese A, Fuganti A. Forging of a MMC for an automotive component. Metall Sci Technol 1996;14: 13–19. Teksid, Torino.
[6] De Sanctis AM, Evangelista E, Forcellese A, Wang YZ. Forging of MMCs. BRITE_EURAM II Report 6; 1996.
[7] Brechet Y, Embury JD, Tao S, Luo L. Acta Metall Mater 1993;39: 1781.
[8] Mummery PM, Derby B, Scruby CB. Acta Metall Mater 1993;41: 1431.
[9] Singh PM, Lewandowski JJ. Metall Trans A 1995;26A:2911.
[10] Lewandowski JJ, Liu C, Hunt WH. Mater Sci Engng A 1989;107:241.
[11] Li C, Ellyin F. Mater Sci Engng 1996;A214:115.
[12] Cerri E, Spigarelli S, Evangelista E, Cavaliere P. Hot deformation and processing maps of a particulate-reinforced 6061 + 20% Al_2O_3 composite. Mater Sci Engng 2002;A324:157–61.
[13] McQueen HJ, Sakaris P, Bowles J. In: Chandra T, Dhingra AK, editors. Advanced composites, vol. 93. Warrendale, PA: The Minerals, Metals and Materials Society; 1993. p. 1193.
[14] McQueen HJ, Ryan ND. Constitutive analysis in hot working. Mater Sci Engng 2002;A322:43–63.
[15] Prangnell PB, Barnes SJ, Roberts SM, Withers PJ. The influence of temperature on microstructural damage during uniaxial compression of aluminium matrix composites. Scripta Metall Mater 1995;33(2): 323–9.
[16] Barnes SJ, Prangnell PB, Humprhreys FJ. Microstructural characterisation as-received, deformed and forged al composites. Brite Euram CEC Contract: BRE2-CT92-0177, Final Report.
[17] Prangnell PB, Barnes SJ, Roberts SM, Withers PJ. The effect of particle distribution on damage formation in particulate reinforced metal matrix composites deformed in compression. Mater Sci Engng 1996;A220:41–56.
[18] Lay B, Brunet M, Boivin M. Modelling of void nucleation and fiber debonding in a composite material. J Mater Product Technol 1998;77: 254–9.
[19] Carrere N, Boivin D, Valle R, Vasse A. Local textures measurements in a SiC/Ti composite manufactured by the foil–fiber–foil technique. Scripta Mater 2001;44:867–72.
[20] Tan M, Xin Q, Li Z, Zong BY. Influence of SiC and Al_2O_3 particulate reinforcements and heat treatments on mechanical properties and damage evolution of Al-2618 metal matrix composites. J Mater Sci 2001;36:2045–53.
[21] Humphreys FJ, Hatherly M. Recrystallization and related annealing phenomena. Amsterdam: Elsevier; 1995.
[22] Dieter GE. Mechanical metallurgy, 3rd ed. New York: McGraw-Hill; 1986.
[23] Sellars CM, Tegart WJMcG. Relation between strength and structure in hot deformation. Mater Sci Rev 1966;63:731–46.
[24] Alunni A, Cerri E, Evangelista E, Forcellese A. Temperature sand strain rate effect on hot formability of 6061 + 20 vol.% SiC whiskers. In: Chandra T, Dhingraa AK, editors. Proceedings of

the International Conference on Advanced Composites Materials (ICACM). Wollongong (Australia): TMS-Minerals, Metals and Materials Society; 1993. p. 1079–85. February 15–19.
[25] Xia X, McQueen HJ, Sakaris P. Hot deformation mechanisms in a 10 vol.% Al_2O_3 particle reinforced 6061 Al matrix composite. Scripta Metall 1995;32:1185–90.
[26] Pickens JR, Langan TJ, England RO, Liebson M. Metall. Trans. 1987; 18A:303.
[27] Forming and Forging, Metal handbook, vol. 4. Metals Park, OH: ASM International; 1988. p. 290–327.
[28] Dieter GE, Metals handbook, vol. 14. Metal Park, OH: ASM; 1987. p. 363.
[29] Xia X, Sakaris P, McQueen HJ. Hot deformation and recrystallization behaviour of a SiCp/6061 Al composite. Proceedings of the Ninth International Conference on Composite Materials (ICCM/9), Madrid; 1993. p. 157–62.
[30] Sellars CM, Tegart WJMcG. Hot workability. Int Mater Rev 1972; 17:1–24.
[31] Spigarelli S, Evangelista E, Cerri E, Langdon TG. Constitutive equations for hot deformation of an Al-6061/20% Al_2O_3 composite. Mater Sci Engng 2001;A319–321:721–5.
[32] Semiatin SL, Lahoti GD, Jonas JJ. Application of the torsion test to determine workability. Mechanical testing, 9th ed. Metals handbook, vol. 8. American Society for Metals; 1985. p. 154–84.
[33] Mc Queen HJ, Evangelista E, Jin N, Kassner ME. Energy dissipation efficiency in aluminium dependent on monotonic flow curves and dynamic recovery. Metall Mater Trans 1995;26A:1757–66.
[34] Alexander JM. In: Lenard JG, editor. Modeling of hot deformation of steels. Berlin: Springer; 1989. p. 101.
[35] Prasad YVRK, Sasidhara S, editors. Hot working guide: a compendium of processing maps. Warrendale, PA: ASM; 1999. p. 25–157.
[36] Prasad YVRK, Seshacharyulu T. Mat Sci Engng 1998;A243:82–8.
[37] Narayana Murty SVS, Nageswara Rao B. Metall Trans 1997;28A: 2170.
[38] Narayana Murty SVS, Nageswara Rao B. Mater Sci Engng 1998; A254:76.
[39] Ziennkiewicz OC, Taylor RL. The finite element method, V.1, V.2.
[40] Ziegler H, Progress in solid mechanics, vol. 4. New York: Wiley; 1963. p. 93.
[41] Stuwe HP. Flow curves of polycristalline metals and their application in plasticity mechanics. Z Metallk 1965;56:633–42.
[42] Hoffmanner AL. The use of workability test results to predict, processing limits, metal forming: interrelation between theory and practice. New York: Plenum Press; 1961. p. 349–91.
[43] Sakai T, Jonas JJ. Acta Metall 1984;32:189.
[44] Doherty RD, Hughes DA, Humphreys FJ, Jonas JJ, Juul Jensen D, Kassner ME, King WE, McNelley TR, McQueen HJ, Rollett AD. Current issues in recrystallization: a review. Mater Sci Engng 1997; A238:219–74.
[45] McQueen HJ, Evangelista E, Bowles J, Crawford G. Met Sci 1984; 18:395.
[46] Humphreys FJ. A unified theory of recovery, recrystallization and grain growth, based on the stability and growth of cellular microstructures. I. The basic model. Acta Mater 1997;45(10): 4231–40.
[47] Humphreys FJ. A unified theory of recovery, recrystallization and grain growth, based on the stability and growth of cellular microstructures. II. The effect of second-phase particles. Acta Mater 1997;45(12):5031–9.
[48] Gourdet S, Montheillet F. Effects of dynamic grain boundary migration during the hot compression of high stacking fault energy metals. Acta Mater 2002;50(11):2801–12. June.
[49] Ko B-C, Yoo Y-C. Prediction of dynamic recrystallization condition by deformation efficiency for Al 2024 composite reinforced with SiC particle. J Mater Sci 2000;35:4073–7.
[50] Yoo Y-C, Jeon J-S, Lee H-I. The effect of SiC whiskers on the hot deformation behaviour of SiCw/AA2124 composites. Compos Sci Technol 1997;57:651–4.
[51] Spigarelli S, Cerri E, Cavaliere P, Evangelista E. An analysis of hot formability of the 6061 + 20% Al_2O_3 composite by means of different stability criteria. Mater Sci Engng 2002;A327:144–54.
[52] Taya M. Strenghthening mechanisms of metal matrix composites. Mater Trans, JIM 1991;32(1):1–19.
[53] Evangelista E, McQueen HJ, Ryan ND. Metal Sci Technol 1991;9:75.
[54] Weissenbek E, Rammerstorfer FG. Influence of the fiber arrangement on the mechanical and thermomechanical behaviour of short fiber reinforced MMCs. Acta Metal Mater 1993;41:2833–43.
[55] Semiatin SL, Jonas JJ, Mecking H. Acta Metall 1979;27:419.